**P1-045**

# Thermal annealing and exposure to divertor-like deuterium plasma of tailored tungsten oxide coatings

**A. Pezzoli**[a]*, D. Dellasega[a,b], V. Russo[a], A. Gallo[a,c], P.A. Zeijlmans van Emmichoven[c], M. Passoni[a,b]

[a] *Dipartimento di Energia, Politecnico di Milano – Milano (Italy).*

[b] *Istituto di Fisica del Plasma, CNR, EURATOM-ENEA-CNR Association – Milano (Italy).*

[c] *FOM Institute DIFFER – Dutch Institute for Fundamental Energy, Association EURATOM-FOM, Partner in the Trilateral Euregio Cluster – Nieuwegein (Netherlands).*

## Abstract

In this work we produced tungsten (W) and W oxide ($WO_x$) films by pulsed laser deposition (PLD) with the aim of the addressing modifications of structure and morphology that occur after annealing treatments and high-flux deuterium plasma. Thanks to the high flexibility of PLD we produced nanostructured W containing non-bounded oxygen, different types of $WO_x$ and multilayered films. W coatings are dense, non-porous and exhibit a nanocrystalline structure, resembling the coatings used as first wall in Tokamaks. The oxide films are nearly stoichiometric amorphous $WO_x$ (x = 3) with different morphology from compact to porous. Depending on annealing temperature, nucleation of different crystalline phases (e.g. $WO_3$, $W_{18}O_{49}$) occurs. Exposure of films to high-flux (~ $10^{24}$ $m^{-2}$ $s^{-1}$) deuterium plasmas in Magnum-PSI at different surface temperatures ($T_{max}$ = 580 K) determines material modifications at the nanoscale (e.g. nanometric defects) but no delamination. In addition preliminary deuterium retention results are reported.

---

*PACS:* 28.52.Fa, 52.40.Hf, 81.15.Fg, 81.05.Je

*PSI-21 keywords:* Coating, Deuterium inventory, Divertor material, Tungsten, Oxidation.

**Corresponding author address:* via Ponzio 34/3, 20133 Milano (Italy).

**Corresponding author E-mail:* andrea.pezzoli@polimi.it

*Presenting author:* Andrea Pezzoli

*Presenting author e-mail:* andrea.pezzoli@polimi.it

## 1. Introduction

Due to its low erosion yield, high melting temperature, high thermal conductivity, low hydrogen isotope permeation and inventory, tungsten (W) is a candidate material for plasma facing components (PFCs) in fusion reactors **[1]**. W is used for PFCs in operating tokamaks (e.g. ASDEX-Upgrade and JET-ILW) and will be used in future devices (e.g. ITER). Despite its suitable properties in tokamak environment, W undergoes several changes, due to neutronic and ionic fluence, temperature and sputtering processes, that produces modifications to bulk W leading to its damaging, erosion, re/co-deposition. In these conditions W shows properties and compositions which can be different from bulk W. It can also form different types of compound materials during re/co-deposition process in presence of buffer (e.g. Nitrogen)[2] and impurity gases (e.g. Oxygen, $O_2$) [3]. Since $O_2$ and oxygen compounds can be present as contaminations in tokamak vacuum vessel, oxidation can occur on PFCs, due to the high temperature reached by components during operation, and eroded material from PFCs can be re-deposited with a different stoichiometry [3,4]. While many studies on W erosion and deuterium ($D_2$) retention and permeation for different kinds of W (e.g. bulk and **W coatings**) are available [5–7], the behavior of tungsten oxide ($WO_x$) in a tokamak environment is not well known. $WO_x$ has different properties from W, such as higher erosion yield [**8**] and different hydrogen isotope retention mechanisms [**9–11]**. In literature, there are only few works in which tungsten trioxide ($WO_3$) coatings have been exposed to $D_2$ plasma. In these works $WO_3$ has been obtained either by thermal annealing in air of bulk W [10,11] or by evaporation of amorphous $WO_3$ coatings later annealed in vacuum up to 870 K [12]. The produced oxide layers are monoclinic, crystalline with

thickness ranging from hundreds of nanometers to microns and limited capability of varying stoichiometry. After exposure to $D_2$ plasma, these coatings exhibit a larger amount of retained $D_2$ if compared with Plasma Spray and CMSII W coatings [13,14] and they show loss of $O_2$ from surface due to chemical reaction of $O_2$ with $D_2$ [15]. These coatings are quite different from oxide layers that could be present in a tokamak because native oxide layers are thinner than hundreds of nanometers and, in addition, an amorphous structure has to be expected. Moreover, also re-deposited $WO_x$ compounds will probably have an amorphous structure with peculiar stoichiometry **[16–19]**. To make major advances in our understandings of these important issues, it is essential to produce, in a controlled way, coatings that are able to simulate native oxide layer, co-deposited $WO_x$ coatings and mixed layer structures. These coatings should be tested in ITER-relevant tokamaks or in linear machines plasma generators able to reproduce conditions that will be present in ITER divertor.

The aim of this work is to produce and test $WO_x$ coatings that are similar to the oxide layers in tokamaks. The capabilities of Pulsed Laser Deposition (PLD) are used to control the properties of the coatings on the nanoscale, i.e., thickness, morphology, structure and stoichiometry [20,21]. The coatings modifications due to annealing treatments are investigated. In addition, exposures to D plasma at divertor-like condition are performed in Magnum-PSI. Preliminary results on $D_2$ post-exposure retention are presented.

## 2. Experimental

Our PLD system exploits a nanosecond laser pulse $2^{nd}$ harmonic of a Nd:YAG laser ($\lambda$=532 nm, pulse duration 5-7 ns, repetition rate 10 Hz) focused on a W target (purity 99.9%). The laser spot is about 9.2 $mm^2$, pulse energy is 815 mJ. The species ablated from the target expand in a proper vacuum chamber (base pressure of $10^{-3}$ Pa), where an $O_2$ background gas (purity 99.999%) is present. $O_2$ pressure ranges between 5 and 100 Pa. The expanding species are collected on a

grounded rotating substrate of Silicon (100) 2.5 mm x 2.5 mm or polycrystalline W substrate (PLANSEE, 99.96% purity, Ø 20 mm, 1 mm thick) containing micrometer-sized grains and mechanically polished until mirror finish. The substrate is 60 mm away from the target at room temperature. Further details are given in a previous work [20].

The films are characterized with a Zeiss Supra 40 field emission scanning electron microscope (SEM, accelerating voltage 5 kV). In order to check film composition, energy dispersive X-ray spectroscopy (EDXS) is performed using an accelerating voltage of 15 kV, to excite $K_\alpha$ and $M_\alpha$ electronic levels of Oxygen (O) and W, respectively. $K_\alpha$ of Cobalt is used for system calibration. Every EDXS analysis is repeated three times on equivalent points of the sample, the number of X-ray counts for each measurement being 250000. The inspected thickness range is around 1 μm (data obtained with CASINO simulation using $WO_3$ bulk density and 15 keV electrons), depending on structural properties of different samples.

Micro-Raman measurements are performed to detect the presence and stoichiometry of $WO_x$, with a Renishaw InVia spectrometer and using the 514.5 nm wavelength of an $Ar^+$ laser.

To better understand $WO_x$ thermal behavior, some specific samples, deposited on W substrates, are annealed in a high-vacuum chamber ($10^{-5}$ Pa) for 1 h using a resistive heater stage. A K-Thermocouple is used to monitor the stage temperature.

$WO_x$ coatings, deposited on W substrates and not annealed, were exposed to high-flux deuterium plasmas in the linear plasma generator Magnum-PSI at FOM-DIFFER [22,23] at low surface temperature (maximum temperature in center of plasma beam of $T_{max}$ = 580 K). The electron density and temperature of the plasma were measured with Thomson scattering [24]. The flux on the target can be estimated by using Bohm criterion [25,**26**], leading to a maximum flux in the center of the plasma beam of $10^{24}$ $m^2$ $s^{-1}$. The targets are subject to 6 plasma shots of 25 s each,

which leads to an average plasma fluence of typically 1 x $10^{26}$ $m^{-2}$. During exposure, the targets are kept at floating voltage.

## 3. Results and Discussions

### *3.1. $WO_x$ films deposition*

In order to obtain films with controlled morphology, structure and stoichiometry, a wide range of pressures (from 5 Pa to 100 Pa of $O_2$) is investigated. In figure 1 an EDXS analysis of the samples as a function of the $O_2$ pressure during deposition is shown. **The O/W ratio in films increases with raising $O_2$ pressure from vacuum ($10^{-3}$ Pa) to 30 Pa and in the end it stabilise at around 3, independently of $O_2$ pressure during deposition.** In figure 2a Raman spectra of the samples deposited at various background $O_2$ pressure are reported. For films deposited in an $O_2$ atmosphere below 30 Pa no Raman signal is detected, revealing their metallic nature. Above 30 Pa of $O_2$, Raman spectra show a low frequency band in the range 100-500 $cm^{-1}$, associated to O-W-O bending modes, a band in the range 600-900 $cm^{-1}$, associated to W−O stretching modes and a band at about 960 $cm^{-1}$ attributed to W=O stretching modes at grain boundaries, therefore related to the presence of nano-grains [21]: this typical broad band feature in Raman spectra implies that the deposited oxide films are nearly stoichiometric amorphous tungsten oxide (a-$WO_3$) [21]. In these spectra a narrow peak at 521 $cm^{-1}$ due to the first order scattering from silicon substrate is also evident: this confirms the optical transparency properties of these films due to their oxide nature. In figure 3 a SEM cross section analysis is reported. The film morphology changes, from compact to porous, varying $O_2$ pressure from 30 Pa to 100 Pa (figure 3a and 3b respectively). In addition, in figure 4a a plain view SEM image of the sample deposited at 30 Pa $O_2$ atmosphere is presented. Furthermore, thanks to the great versatility of PLD, multi-layer structures have also been deposited: in figure 3c, the dark layer on the top of a

nanostructured columnar W film (c-W) is a thin a-$WO_3$ layer (50 nm), while figure 3d shows a similar a-$WO_3$ film buried between two c-W layer.

Different types of W and $WO_3$ coatings, with an high thickness control, can be produced using PLD: in particular, the deposition of metallic W films with a controlled amount of not bonded O is achievable below a threshold pressure (30 Pa). It is feasible to obtain various morphologies of a-$WO_3$, from compact to porous, above 30 Pa, by tuning pressure during deposition. Finally, the oxide layer can be put in multi-layer structures, which can be useful for simulating different kinds of co-redeposited coatings that could be present on PFCs.

For the aims of this work, 30 Pa $O_2$ atmosphere is selected as reference pressure to produce compact a-$WO_3$ films, than can mimic $WO_x$ co-redeposition present in tokamak environment, with a thickness of 1 μm, high uniformity and planarity for subsequent analysis.

*3.2. Annealing*

The expected working conditions in the ITER divertor involve temperatures ranging from about 400 K to 1150 K [27,28] and high vacuum (~ $10^{-3}$ Pa). To better understand a-$WO_3$ thermal behavior, films deposited at 30 Pa $O_2$ have been annealed in vacuum for 1 h at 570 K, 870 K and 1150 K. It is interesting to note that at 1150 K $WO_3$ starts to volatilize even in air [15]. The film deposited at room temperature and the one annealed at 570 K keep the same surface morphology (figure 4a) and structure (Raman spectrum (2) in figure 2b and Raman spectrum (30 Pa) in figure 2a). These results show that, below 570 K, a-$WO_3$ is not subjected to modifications induced by temperature. At higher temperature, modifications occur. In figure 4b a plain SEM view of a sample annealed at 870 K is reported. In this case, morphology modifications are evident, such as cracks that interrupt film continuity. Raman spectrum (3) in figure 2b presents narrow peaks at 135 $cm^{-1}$, 270 $cm^{-1}$, 721 $cm^{-1}$ and 812 $cm^{-1}$, showing that, at this temperature, a-$WO_3$ crystallizes as monoclinic $WO_3$ [29,**30**]. In figure 4c SEM plain view of a film annealed at 1150 K is

reported; an evident morphological modification occurs with nano-rods and nano-sheets growing on the surface sample. These morphological features, together with the very complex peaks pattern reported in the Raman spectrum (4) in figure 3b, attest the formation of the Magneli phase, that is a sub-stoichiometric phase of $WO_3$, defined as $W_{18}O_{49}$ (or $WO_{2,75}$) [29,**31**]: the decrease in the O content is caused by the annealing treatment at 1150 K in vacuum.

*3.3. Magnum-PSI exposure*

In figure 4d, a SEM plain view of the sample deposited at 30 Pa $O_2$ and exposed to D plasma at 580 K films is reported. Surface modifications occur, such as nano-cracks and point-like features. The Raman signal dramatically decreases (spectrum (1) in figure 2b) pointing out loss of O from the film, probably due to the reduction reaction that occurs between $WO_x$ and D during plasma exposure. It is known that reduction of $WO_3$ by $H_2$ starts at around 850 K [15]; in the Magnum-PSI plasma, $D_2$ is present in dissociated and ionized form (D) and this probably allows the reduction starting at lower temperatures. In the exposed sample, the O/W ratio, as obtained with EDXS, is about 2.5, confirming the O loss. Thermal desorption spectroscopy (TDS) has been performed to investigate the retention of deuterium in the thin films. The TDS signal of $D_2$ for the 1 μm a-$WO_3$ film exposed to D plasma is displayed in figure 5, together with the TDS signal for the 1 μm c-W film exposed at similar conditions. The spectrum of the a-$WO_3$ film shows the presence of two desorption peaks at 500 K and 780 K, while the c-W film shows a broad TDS spectrum with its maximum at about 580 K and a shoulder at higher temperatures. The small peak at ~700 K is most likely caused by an experimental artifact during the heating procedure. The total number of D atoms desorbed from the a-$WO_3$ film is 6.1 x $10^{19}$ D $m^{-2}$, which is a factor 20 lower than 1.3 x $10^{21}$ $m^{-2}$ for the c-W film. These total numbers include the deuterium desorbing as HD **but not the contribution due to heavy waters (HDO and $D_2O$) desorption. For this reason values reported can be affected to an underestimation of total D retained**.

Nevertheless, it should be noted that whereas the total deuterium desorption for the c-W is dominated by $D_2$, for the oxide film the $D_2$ signal is a factor of 1.4 smaller than the HD signal. Moreover D retained in a-$WO_3$ coating is 2 times lower than D retained in monoclinic thermally grown $WO_3$ [10].

## 4. Conclusions

$WO_x$ films were deposited using PLD technique **in order to simulate re-deposited compound layers that can be present onto PFCs.** It is shown how films morphology and stoichiometry can be controlled changing background $O_2$ during deposition. Two different growth regimes are determined with SEM and Raman analysis. In particular, below 30 Pa $O_2$ metallic W films are deposited, with different concentrations of not bonded O depending on background deposition pressure; above 30 Pa, a-$WO_3$ films with different morphologies, from compact to porous, are obtained. Compact a-$WO_3$ films have been annealed in vacuum at different temperatures to investigate their thermal behavior: at 570 K no changes are observed; at 870 K monoclinic phase of $WO_3$ is formed; at 1150 K Magneli phase ($W_{18}O_{49}$) is obtained. 1μm compact a-$WO_3$ film and 1 μm c-W film are exposed to high-flux D plasma in Magnum PSI at low temperature. After exposure, a-$WO_3$ exhibits changes, such as loss in O content and nano-defects. Comparison between $D_2$ retention in c-W and a-$WO_3$ highlights that retention in oxide film is 20 times lower than that in c-W.

In the future, different oxide coatings will be tested in plasma simulators (e.g. Magnum PSI) or in tokamaks, to better understand their retention properties.

**Acknowledgements**

The authors wish to thank G. Granucci, G. Grosso, M. Lontano. Part of this work is supported by the European Communities under the contract of Association EURATOM/ENEA-CNR. The

views and opinions expressed herein do not necessarily reflect those of the European Commission.

**References**


[1] T. Tanabe, N. Noda, H. Nakamura, J. Nucl. Mater. 196-198 (1992) 11.

[2] A. Kallenbach, M. Balden, R. Dux, T. Eich, C. Giroud, A. Huber, G.P. Maddison, M. Mayer, K. McCormick, R. Neu, T.W. Petrie, T. Pütterich, J. Rapp, M.L. Reinke, K. Schmid, J. Schweinzer, S. Wolfe, J. Nucl. Mater. 415 (2011) S19.

[3] J.P. Coad, E. Alves, N.P. Barradas, a Baron-Wiechec, N. Catarino, K. Heinola, J. Likonen, M. Mayer, G.F. Matthews, P. Petersson, a Widdowson, Phys. Scr. T159 (2014) 014012.

[4] R. Neu, C. Hopf, a. Kallenbach, T. Pütterich, R. Dux, H. Greuner, O. Gruber, a. Herrmann, K. Krieger, H. Maier, V. Rohde, J. Nucl. Mater. 367-370 (2007) 1497.

[5] S. Brezinsek, T. Loarer, V. Philipps, H.G. Esser, S. Grünhagen, R. Smith, R. Felton, J. Banks, P. Belo, a. Boboc, J. Bucalossi, M. Clever, J.W. Coenen, I. Coffey, S. Devaux, D. Douai, M. Freisinger, D. Frigione, M. Groth, a. Huber, J. Hobirk, S. Jachmich, S. Knipe, K. Krieger, U. Kruezi, S. Marsen, G.F. Matthews, a. G. Meigs, F. Nave, I. Nunes, R. Neu, J. Roth, M.F. Stamp, S. Vartanian, U. Samm, Nucl. Fusion 53 (2013) 083023.

[6] M.H.J. 't Hoen, M. Mayer, a. W. Kleyn, H. Schut, P. a. Zeijlmans van Emmichoven, Nucl. Fusion 53 (2013) 043003.

[7] V. Nemanič, B. Zajec, D. Dellasega, M. Passoni, J. Nucl. Mater. 429 (2012) 92.

[8] J. Roth, J. Bohdansky, W. Ottenberger, Data on Low Energy Light Ion Sputtering, Max-Planck-Inst. für Plasmaphysik, 1979.

[9] S. Nagata, K. Takahiro, Phys. Scr. 106 (2001).

[10] V.K. Alimov, V. Sharapov, A. Gorodetsky, Phys. Scr. T103 (2003) 72.

[11] V.K. Alimov, B. Tyburska, M. Balden, S. Lindig, J. Roth, K. Isobe, T. Yamanishi, J. Nucl. Mater. 409 (2011) 27.

[12] O.V. Ogorodnikova, J. Roth, M. Mayer, J. Nucl. Mater. 313-316 (2003) 469.

[13] O. V. Ogorodnikova, T. Schwarz-Selinger, K. Sugiyama, V.K. Alimov, J. Appl. Phys. 109 (2011) 013309.

[14] O. V. Ogorodnikova, T. Schwarz-Selinger, K. Sugiyama, T. Dürbeck, W. Jacob, Phys. Scr. T138 (2009) 014053.

[15] E. Lassner, W. Schubert, Tungsten: Properties, Chemistry, Technology of the Elements, Alloys, and Chemical Compounds, Springer, New York, 1999.

[16] M. Psoda, M. Rubel, G. Sergienko, P. Sundelin, a. Pospieszczyk, J. Nucl. Mater. 386-388 (2009) 740.

[17] M.J. Rubel, G. Sergienko, a. Kreter, a. Pospieszczyk, M. Psoda, E. Wessel, Fusion Eng. Des. 83 (2008) 1049.

[18] M. Balden, N. Endstrasser, P.W. Humrickhouse, V. Rohde, M. Rasinski, U. von Toussaint, S. Elgeti, R. Neu, Nucl. Fusion 54 (2014) 073010.

[19] A. Litnovsky, M. Matveeva, A. Herrmann, V. Rohde, M. Mayer, K. Sugiyama, K. Krieger, V. Voitsenya, G. Vayakis, A.E. Costley, R. Reichle, G. De Temmerman, S. Richter, U. Breuer, L. Buzi, S. Möller, V. Philipps, U. Samm, P. Wienhold, Nucl. Fusion 53 (2013) 073033.

[20] D. Dellasega, G. Merlo, C. Conti, C.E. Bottani, M. Passoni, J. Appl. Phys. 112 (2012) 084328.

[21] F. Di Fonzo, a. Bailini, V. Russo, a. Baserga, D. Cattaneo, M.G. Beghi, P.M. Ossi, C.S. Casari, a. Li Bassi, C.E. Bottani, Catal. Today 116 (2006) 69.

[22] J. Scholten, P. a. Zeijlmans van Emmichoven, H.J.N. van Eck, P.H.M. Smeets, G.C. De Temmerman, S. Brons, M. a. van den Berg, H.J. van der Meiden, M.J. van de Pol, M.F. Graswinckel, P.W.C. Groen, a. J. Poelman, J.W. Genuit, Fusion Eng. Des. 88 (2013) 1785.

[23] H.J.N. van Eck, a. W. Kleyn, a. Lof, H.J. van der Meiden, G.J. van Rooij, J. Scholten, P. a. Zeijlmans van Emmichoven, Appl. Phys. Lett. 101 (2012) 224107.

[24] H.J. van der Meiden, a R. Lof, M. a van den Berg, S. Brons, a J.H. Donné, H.J.N. van Eck, P.M.J. Koelman, W.R. Koppers, O.G. Kruijt, N.N. Naumenko, T. Oyevaar, P.R. Prins, J. Rapp, J. Scholten, D.C. Schram, P.H.M. Smeets, G. van der Star, S.N. Tugarinov, P. a Zeijlmans van Emmichoven, Rev. Sci. Instrum. 83 (2012) 123505.

[25] P.C. Stangeby, The Plasma Boundary of Magnetic Fusion Devices, IOP, Philadelphia, 2000.

[26] A. Guthrie, R.K. Wakerling, The Characteristics of Electrical Discharges in Magnetic Fields, McGraw-Hill, New York, 1949.

[27] J.N. Brooks, J.P. Allain, R.P. Doerner, a. Hassanein, R. Nygren, T.D. Rognlien, D.G. Whyte, Nucl. Fusion 49 (2009) 035007.

[28] T. Hirai, G. Pintsuk, Fusion Eng. Des. 82 (2007) 389.

[29] A. Ponzoni, V. Russo, A. Bailini, C.S. Casari, M. Ferroni, A. Li Bassi, A. Migliori, V. Morandi, L. Ortolani, G. Sberveglieri, C.E. Bottani, Sensors Actuators B Chem. 153 (2011) 340.

[30] J. Gabrusenoks, A. Veispals, A. von Czarnowski, K.-H. Meiwes-Broer, Electrochim. Acta 46 (2001) 2229.

[31] G.L. Frey, A. Rothschild, J. Sloan, R. Rosentsveig, R. Popovitz-Biro, R. Tenne, J. Solid State Chem. 162 (2001) 300.

**Figure captions**

Figure 1. Elemental composition: Oxygen on Tungsten ratio (O/W) calculated using EDXS versus deposition background $O_2$ pressure.

Figure 2. (a) Raman spectra of the films deposited on Silicon substrates varying background $O_2$ pressure (star marker indicates Silicon peak at 521 $cm^{-1}$); (b) Raman spectra of the film deposited on W substrate at 30 Pa $O_2$ background pressure annealed at 570 K (2), 870 K (3), 1150 K (4) and exposed at 580 K D plasma (1).

Figure 3. SEM cross section analysis of a-$WO_3$ films deposited varying $O_2$ deposition pressure (a)-(b) and multi-layer films (W + $WO_x$) (c)-(d).

Figure 4. SEM plain view of the a-$WO_3$ films deposited in 30 Pa $O_2$ background atmosphere: at room temperature and annealed at 570 K (a), annealed at 870 K (b) at 1150 K (c) and exposed to 580 K $D_2$ plasma in Magnum-PSI (d).

Figure 5. TDS Spectrum of 1 μm a-$WO_3$ and of 1 μm c-W, deposited in 30 Pa $O_2$ background pressure and vacuum ($10^{-3}$ Pa) respectively, exposed to 580 K D plasma (signal related to mass 4, $D_2$).

**Figures**

Figure 1.

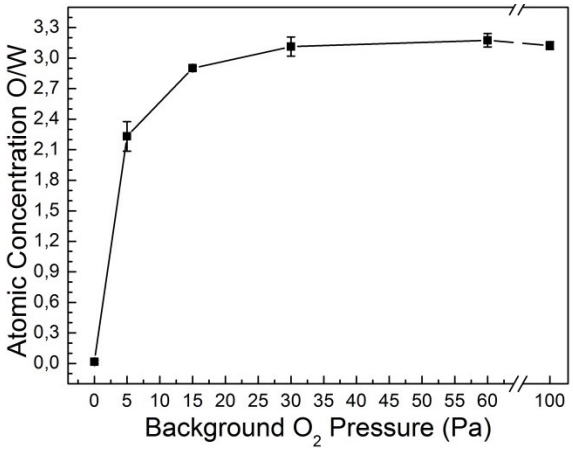


Figure 2.

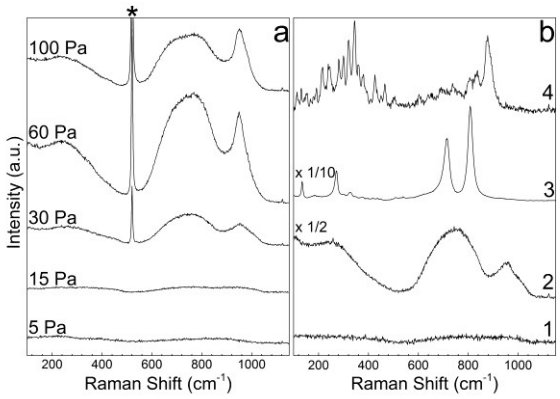


Figure 3.

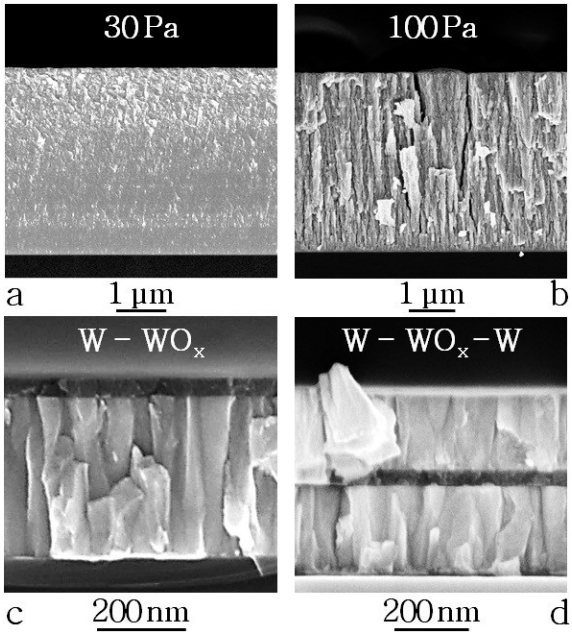

Figure 4.

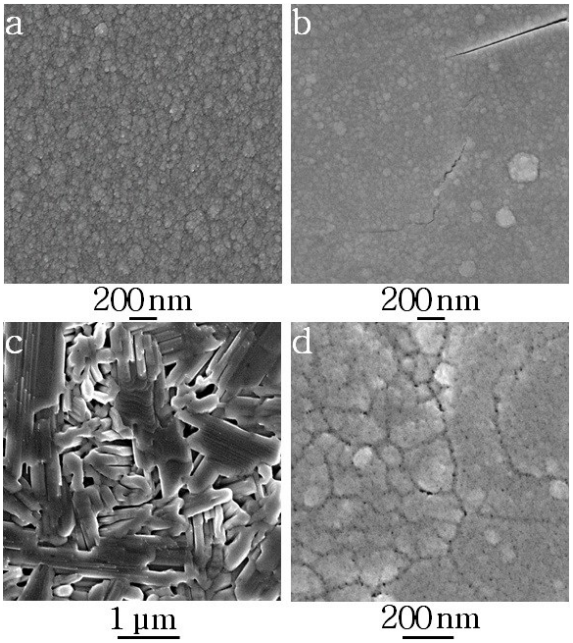


Figure 5.